Review

J. Mex. Chem. Soc. **2023**, *67*(4)
Special Issue

ISSN-e 2594-0317

Why Measure Particle-by-Particle Electrochemistry? A Tutorial and Perspective

Salvador Gutierrez-Portocarrero[1], Mario A. Alpuche-Avilés[2]*

[1]Current address: Department of Chemistry, University of Utah, USA.
[2]Department of Chemistry, University of Nevada, Reno, Nevada 89557, USA.

***Corresponding author:** Mario A. Alpuche-Avilés, email: malpuche@unr.edu

Received March 23rd, 2023; Accepted June 10th, 2023.

DOI: http://dx.doi.org/10.29356/jmcs.v67i4.2014

This paper is dedicated to Dr. Ignacio González Martínez as part of the JMCS special issue "Tribute to emeritus SNI Researchers in the area of electrochemistry."

Abstract. Single-particle electrochemistry has become an important area of research with the potential to determine the rules of electrochemical reactivity at the nanoscale. These techniques involve addressing one entity at the time, as opposed to the conventional electrochemical experiment where a large number of molecules interact with an electrode surface. These experiments have been made feasible through the utilization of ultramicroelectrode (UMEs), i.e., electrodes with at least one dimension, e.g., diameter of 30 μm or less. This paper provides a theoretical and practical introduction to single entity electrochemistry (SEE), with emphasis on collision experiments between suspended NPs and UMEs to introduce concepts and techniques that are used in several SEE experimental modes. We discuss the intrinsically small currents, below 1 nA, that result from the electroactive area of single entities in the nanometer scale. Individual nanoparticles can be detected using the difference in electrochemical reactivity between a substrate and a nanoparticle (NP). These experiments show steady-state behavior of single NPs that result in discrete current changes or steps. Likewise, the NP can have transient interactions with the substrate electrode that result in current blips. We review the effect of diffusion, the main mass transport process that limits NP/electrode interactions. Also, we pointed out the implications of aggregation and tunneling in the experiments. Finally, we provid a perspective on the possible applications of single-element electrochemistry of electrocatalyst.
Keywords: Single-entity electrochemistry; nano-impact; nanoelectrochemistry; electroactivity; electrocatalysis.

Resumen. La electroquímica de partículas individuales se ha convertido en un área importante de investigación con el potencial de facilitar la comprensión de las reglas de reactividad electroquímica en la escala de nanómetros. Estas técnicas implican abordar una entidad a la vez, en contraste con el experimento electroquímico convencional en el que un gran número de moléculas interactúa con la superficie de un electrodo. Estos experimentos se han vuelto posibles gracias al uso de ultramicroelectrodos (UME, por sus siglas en inglés), es decir, electrodos con al menos una dimensión, como, por ejemplo, el diámetro de 30 μm o menos. Este artículo proporciona una introducción teórica y práctica a la electroquímica de entidad única (SEE, por sus siglas en inglés), con énfasis en los experimentos de colisión entre nanopartículas (NPs) suspendidas y

J. Mex. Chem. Soc. **2023**, *67*(4)
Special Issue

ISSN-e 2594-0317

UME para introducir conceptos y técnicas utilizadas en varios modos experimentales de SEE. Discutimos las corrientes intrínsecamente pequeñas, por debajo de 1 nA, que resultan de la superficie electroactiva de entidades únicas en la escala de nanómetros. Las nanopartículas individuales pueden detectarse mediante la diferencia en reactividad electroquímica entre el sustrato y las nanopartículas. Estos experimentos muestran el comportamiento en estado estacionario de NPs individuales que resulta en cambios discretos de corriente o escalones. De manera similar, la NP puede tener interacciones transitorias con el electrodo de sustrato que dan lugar a picos de corriente. Revisamos el efecto de la difusión, el principal proceso de transporte de masa que limita las interacciones NP/electrodo. Además, señalamos las implicaciones de la agregación y del efecto túnel cuántico en los experimentos. Finalmente, ofrecemos una perspectiva sobre las posibles aplicaciones de la electroquímica de entidad única en electrocatálisis.
Palabras clave: Electroquímica de una sola entidad; nano impacto; nanoelectroquímica; electroactividad; electrocatálisis.

Introduction

Single entity electrochemistry has been considerably developed in the past two decades and has provided novel information not available from bulk or ensemble measurements. However, there are some instrumentation limitations and reproducibility issues that need to be resolved for this area of electrochemistry to be more widely used. These limiting aspects also constitute some areas of opportunity for developing the technique and its application to analytical problems.

Single-entity experiments have gained attention because they provide ways to study electrochemistry at the nanoscale. In general, "bulk" electrochemical experiments deal with a larger number of molecular entities. For example, if the measured current, *i*, from a one electron, *n=1*, faradaic process is 1 µA for a commercially available glassy carbon disk electrode of 3 mm diameter, area, A, around 0.0707 cm^2, then the $Flux = j$, is:

$$j = \frac{i}{nFA} \tag{1}$$

$j = 1.5 \times 10^{-10} mol\ s^{-1} cm^{-2}$. Thus, converting the rate from mol to the number of molecules using Avogadro's number, one obtains $8.8 \times 10^{13}\ molecules \cdot s^{-1} cm^{-2}$. Multiplying the molecular flux by the area, we get the number of molecules electrolyzed per second, which is $6 \times 10^{12}\ molecules/s$ for somewhat typical electrode and solution. The number is approximately $10^{12}\ molecules$ per second being reduced or oxidized on the disk electrode, which is far from a single entity measurement. Thus, measurements such as cyclic voltammetry (CV) on millimeter-diameter disk electrodes under similar flux conditions correspond to thermodynamic ensemble measurements.

In contrast, in single entity measurements, the electrode interrogates one entity at a time. These experiments are analogous to fluorescence single molecule measurements, widely used in biological studies. Similarly, single NP measurements are beginning to yield results that would otherwise be masked in ensemble experiments, such as in the case of NPs. [1]

Hence, the electrode interrogates one entity at a time through different experiments, which are generally denoted with a newly-coined termed *single entity electrochemistry* (SEE) [2,3]. The term *stochastic electrochemistry* was coined to describe collision experiments that involve the interrogation of individual nanoparticles (NPs) through discrete electrochemical signals generated by NP/electrode interactions. These interactions occur when NPs suspended in a solution collide with an ultramicroelectrode (UME). Because NP diffusion through solution usually limits the NP/electrode collision rate, the collisions are non-deterministic in terms of the time between collisions, or in the current that results from a NP/electrode collision. Hence, "stochastic electrochemistry" was used to emphasize the statistical distribution of NP size and the stochastic trajectory.

J. Mex. Chem. Soc. **2023**, *67*(4)
Special Issue

ISSN-e 2594-0317

Single entity electrochemistry modes

Several examples exist of single entity experiments, and their names and detection mode vary; here we present a few of these modes to help us illustrate experimental challenges. Some authors consider the first type of single molecule the patch clamp conductance measurements on single ion channel [4]. However, the use of faradaic currents to detect single molecules or single entities will come later. While the electrochemistry of colloids dates back to 1929 [5] with the goal of making composite materials, more fundamental work included studies of charge transfer in suspended semiconductors [6-8] and the polarography of Heyrovsky of different materials. [9-11] However, in this prior work on colloids, the goal was not to resolve the contributions of individual entities or particles. Later, liposomes were studied one collision at the time, [12] and the electrochemistry of a single molecule was reported, [13] but it was the work of Lemay [14] and Bard [15] that became seminal to the current interest in SEE.

Although single-molecule measurements have been reported with electrochemical feedback conditions [13,16-20] most single entity experiments refer to interrogating one entity, such as a nanoparticle [21-27], a colloidal droplet [28-31], or agglomerates [32-37] of NPs at a time. Single-particle collision experiments have been developed on "hard" spheres including metal NPs (Pt, Au, Cu, Ag) [38-42] and metal oxides (IrO_2, TiO_2, ZnO) [35,43-45]. There are also reports that have shown nano-impact events through the collisions of "soft" particles (micelles) with an UME and an applied electrochemical potential. [28-30,46-50] There are several reviews on the subject, [51-60] but in this paper, we focus on introducing critical concepts and techniques related to nanoparticles or other entities colliding with a working UME. Other modes that are not addressed in depth here, are based on scanning probes techniques and instrumentation, such as such scanning electrochemical microscopy, SECM, [23,24] and scanning electrochemical cell microscopy, SECCM. [26].

Electrocatalytic amplification

These single nanoparticle (NP) experiments rely on large differences on the electrocatalytic properties of the NP material, and the UME with which the NP collides during the experiment. For example, the reaction rate at a surface of a Pt NP for H^+ reduction to H_2 is orders of magnitude larger than the rate at a carbon ultramicroelectrode (UME) surface, so the current recorded is the result of proton reduction "turning on" as a Pt NPs arrive to an essentially inert surface. The H^+ reduction or HER is:

$$2H^+ + 2e^- \xrightarrow{k_i} H_2 \qquad (2)$$

Where k_i, is the electrochemical rate constant (cm/s), and the subscript *i* denotes that the rate constant is different from the NP and the working electrode. In their first report, Xiao and Bard[15] discussed the difference in current and flux between a Pt NP, which is an efficient hydrogen evolution catalyst, colliding with C, where reaction (2) is sluggish, and therefore, the current for HER is often negligible. Other reactions such as H_2O_2 reduction and hydrazine oxidation were also demonstrated for electrocatalytic amplification. [15,42].

Fig. 1 shows two general types of response: step (or staircase) and blip (or spikes) signal. The collisions correspond to NPs. Fig. 1**(a)** shows the current staircase obtained in an experiment with Pt NPs for the oxidation of hydrazine. Once the NPs collide and adsorbed irreversibly to the Au electrode, we observe a discrete increment in the current assigned to a single Pt NP colliding with a Au UME. The Au UME is considered "inert" at the applied potential. Fig. 1**(b)** shows what was originally termed a "blip response", i.e., peaks that are assigned to water oxidation by IrOx particles suspended in solution. Every current blip is assigned to IrOx NPs adsorbing reversibly onto a Pt UME, and once the NPs leave, the current returns to the baseline.

J. Mex. Chem. Soc. **2023**, *67*(4)
Special Issue

ISSN-e 2594-0317

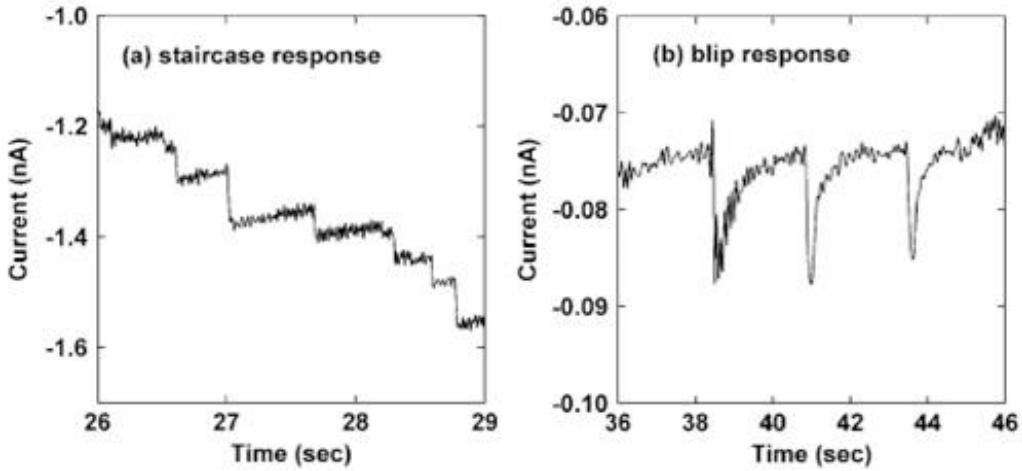

Fig. 1. Stochastic collisions of different types of transient response **(a)** current step for Pt NPs oxidizing hydrazine. Every step in the current is assigned to a single Pt NP colliding with a Au UME which is innert at the applied potential. **(b)** "blip response" for water oxidation by IrOx. Every blip is assigned to IrOx NPs adsorbing reversibly onto a Pt UME. Reproduced with permission from *Phys. Chem. Chem. Phys.,* **2011**, *13*, 5394–5402, The Royal Society of Chemistry.

Several groups study NPs via electrocatalytic amplification upon nanoparticle contact with the electrode, using other reactions, where the NP material is more active—as compared with the working electrode material—towards the electrocatalytic chemical reaction.

In another experimental mode, the adsorption and strong interaction of materials or immiscible phases have been detected using *"blocking collisions"*. [61-63] Blocking experiments and other experimental modes have been used to study soft materials, e.g., ref [61].

The blocking technique provides a wide range of physical phenomena that can be explored, like adsorption, wettability of droplet reactors, and as markers of reactions either in the three-phase boundary or in one phase limited reaction (electrochemistry inside the droplet). A third mode of single entity experiments are the "*nanoimpacts*" [64-69], where the NP material gets electrolyzed or electrotransformed. This mode can provide concentration measurements of NPs in suspension and can allow Ag NPs to be used as tags for the detection of analytes. Also, it has generated methods to analyze water with colloidal mixtures from industrial waste, with high sensitivity, measuring down to zeptomolar concentrations. [70]

Experimental considerations

Experimentally, ultramicroelectrodes, nano-electrodes or other configurations, like SECM, [23,24] SECCM,[26] and the use of nanoband electrodes [71] can provide resolution down to single particle or entities, including single molecules. In collision experiments, detecting single NPs require transient measurement, which often relies on open circuit potential [72-74] as a function of time and chronoamperometry[31,35,40,41,50,75-79]. In the scanning probe techniques, SECM and SECCM, the detection depends on the "contrast", or the ability to discriminate the contribution of an electroactive entity against the background. On the other hand, electrocatalytic amplification, nano-impacts and the heterogeneous interface of electrode-solution-NP are performed generally by chronoamperometry. However, the currents are intrinsically small because they typically correspond to very small surface areas, or to the electrolysis of small number of atoms within NPs. For example, in stochastic collisions, the magnitude of the current transient can be used to determine that the impacts are due to single NPs. The NP on the electrode surface can be approached with the diffusion-limited current for a particle supported on a partially blocking substrate that will give a steady-state current, $i_{d,l}$, given by: [80]

J. Mex. Chem. Soc. **2023**, *67*(4)
Special Issue

ISSN-e 2594-0317

$$i_{d,l} = 4\pi\ ln2\ nDC^{*}r_{NP} \quad (3)$$

For example, in a typical electrocatalytic amplification experiment, it is usual to measure currents in the order of ≲ 50 pA. Note that depending on the conditions, equation (3) can apply for SECM and SECCM.

For nanoimpacts, a current blip is typically assigned to the oxidation of a single NP, and depending on size, kinetics, and other factors, the current can vary from ~ 100 pA to nanoamps. [58] One procedure to determine the size of Ag NPs involves applying a potential positive enough to oxidize the NP so that the reaction is: [81]

$$Ag \rightarrow Ag^{+} + e^{-} \quad (4)$$

The experiment must be able to resolve the discrete current blip that result from the NPs arriving to the working electrode. Then, assuming that the NP was completely oxidized during the collisions, assuming a spherical NP, one can relate the integrated charge of the current peak to the radius: [81]

$$Q_{max} = \frac{4nF\pi\rho r_{NP}^{3}}{3A_r} \quad (5)$$

where r is the NP radius, Q_{max} is the maximum transferred charge (or the total for one current blip), n is the number of electrons for the electrolysis of the NP, so for Ag, n =1 as in eq. (5), ρ is the density, F is Faraday's constant, and A_r is the relative atomic mass. This equation works for smaller NPs, e.g., 50 nm or less, although complications can introduce errors, especially for larger NPs. [58]

Therefore, enhancing the signal-to-noise ratio is often a goal, either by designing a new detection mechanism or through noise discrimination using analog or digital filtering methods. [65,82-84]

Some electrochemical transients due to single entities are defined by changes in current in relatively small times, with commercial instrumentation allowing routine work in the time scale of milliseconds. For faster processes, the ability to resolve them is commonly limited by the electrochemical instrumentation [33,82,85]. Changes that happen in less than μs correspond to relatively higher frequencies. Hence, the signal of interest competes with random noise and nonfaradaic processes or low frequency electrochemical processes in the background from trace species. [86] In addition, diffusional current and charging current decays, double layer changes, are among the processes that compete with the desired signal within the limitation of the instrument. To minimize complications, the experimental setups are commonly selected with an "inert" substrate with a low background, which means that only upon the addition of NPs there will be a significant change in the electrode current.

Nanoparticle diffusion

Fundamentally, a NP in the electrochemical cell will be in Brownian motion until collision with the electrode. The intersection between the NP and the UME will result in a current change at the UME. Depending on the nature of the interaction, the UME will influence the NP diffusion. For example, in the "sticking" collisions, where the NP adsorbs irreversibly to the electrode surface, the electrode will act as a NP sink. Similarly, for nano-impacts, the material dissolution will result in a current decay, where at the end of the experiment there is no NP at the electrode/solution boundary since it would be electrolyzed, e.g., Ag oxidized to Ag^{+}. Under experimental conditions where migration can be neglected, the movement of the NP towards the electrode would follow a Brownian motion. Fig. 2 illustrates the path of a NP in solution that eventually reaches the electrode surface. This simulation is provided to depict the multiple paths that a single NP can have in solution with a diffusion time of 1 ms to represent the NP displacement in the micrometer scale. This scale is closer to what we can measure experimentally in routine electrochemical experiments. As we will discuss below, to be more accurate, the NP should be modeled in steps of ca. 0.2 nm, or time increments of 1 ns.

J. Mex. Chem. Soc. **2023**, *67*(4)
Special Issue

ISSN-e 2594-0317

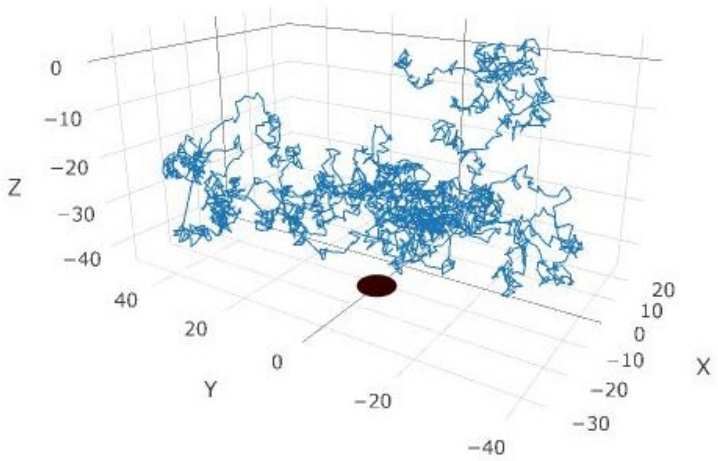

Fig. 2. Schematic of a Brownian motion of a NP. Working disk electrode on the bottom of the xy-plane. The axis scales are in μm.

The Brownian motion simulations where done in R studio following the treatments of Bard and coworkers [87] and White and coworkers [88]. Briefly, we generate the code following three building blocks for the simulations:

1. In the x-axis each particle can move a step to the right or left once every t time interval, moving at velocity $\pm v_x$ a distance d_x. At the same transition time, a particle moves along the y- and z-axis in the same way. In practice, these parameters depend on the size of the particle, the structure of the liquid, and the absolute temperature, T. This condition in a simulation is constrained by defining independent x,y,z movement coordinates, and adding it in a displacement vector $r = \{x, y, z\}$.
2. We consider that the Brownian motion is a process with continuous simple paths that has both stationary and independent normally distributed (Gaussian) increments: If $t_0 = 0 < t_1 < t_2 < \cdots < t_n$. Then the random variables $B(t_i) - B(t_i - 1),\ i \in 2\{1, .., n\}$, are independent with $B(t_i) - B(t_i - 1) \sim N\big(0, (t_i - t_{i-1})\big)$. Therefore, the expected value of δ us $E(\delta)$ and $Var(\delta) = 1$. Thus, we generate the displacement vector with a gaussian random number generator, like, $r = \{rnorm(N, 0,1), rnorm(N, 0,1), rnorm(N, 0,1)\}$.
3. We simulate one particle at a time, which makes the simulations more relevant to conditions where each particle moves independently of the other particles and they do not interact.

Although the simulation in Fig. 2 is only to illustrate NP diffusion, to match the simulation results to the experimental values, we require a method to fix d and t. One can use the v_{RMS}, root-mean-square velocity, and *D*, the NP diffusion coefficient, with equation 6 and 7 to estimate the minimum values of the simulation parameters. [87]

$$\tau = \frac{6D}{v_{RMS}^2} \tag{6}$$

$$\delta = \frac{6D}{v_{RMS}} \tag{7}$$

Moreover, the calculated value of δ and τ are about 0.19 nm and 1 ns respectively for most of the experimental values in the literature. [87] However, we set up the diffusion time to 1 ms and 0.5 μm. We ended the simulation once the Brownian motion of the particle resulted in a collision with the UME. One interesting

J. Mex. Chem. Soc. **2023**, *67*(4)
Special Issue

ISSN-e 2594-0317

feature, that one should keep in mind when interpreting the data and relating it to simulations, is that current changes can be detected when the NP is within tunneling distance while moving in the vicinity of the electrode, as we will discuss below.

NP-electrode collisions

Diffusion-limited frequency

On of the limiting cases of mass transport towards the electrode is the diffusion-limited flux of NPs. In this case, the UME behaves as a sink of NPs with a Dirichlet boundary condition: $C_{NP}^{pca} = 0$ where C_{NP}^{pca} is the averaged concentration of NPs at the electrode surface (or plane of closest approach) and C_{NP}^{*} is the average bulk concentration of particle. The diffusional frequency of NP collisions, $f_{p,d}$, is the product between the diffusional flux, J_d, and the cross-sectional surface, A, of the UME, equation 8. [76]

$$f_{p,d} = J_d \cdot A \tag{8}$$

Expanding the flux, J_d, we obtain equation 9.

$$f_{p,d} = AmC_{NP}^{*} \tag{9}$$

In equation 9, all terms are as previously stated. This equation and the mass transfer coefficient in the literature [89-91] yields the three general diffusion-limited frequencies for each UME geometry. Any frequency of diffusing NP collisions can be calculated knowing the mass transfer coefficient, m, and the geometry of the UME, and the assumption that the electrode acts as a NP sink. Therefore, using the geometrical diffusion limited mass transfer coefficient for UMEs cases of the embedded disk, [92] the hemisphere and sphere, [93-95] the diffusion-limited collision frequencies are (equation 10), (equation 11), and (equation 12), respectively.

$$f_{p,d} = 4D_{NP}r_{WE}C_{NP}^{*} \quad \text{(disk)} \tag{10}$$

$$f_{p,d} = 2\pi D_{NP}r_{WE}C_{NP}^{*} \quad \text{(hemisphere)} \tag{11}$$

$$f_{p,d} = 4\pi D_{NP}r_{WE}C_{NP}^{*} \quad \text{(sphere)} \tag{12}$$

Note that equations (10) to (12) provide the basis of using NP/electrode collision frequency to measure concentration of NPs in suspension if all other parameters are known. The electrode radius is usually available, and D_{NP} can be estimated or measured with dynamic light scattering.

In all stochastic electrochemistry experiments, there are three main experimental features including (i) frequency of collisions onto the UME, and in addition, (ii) the magnitude of the transient, integrated charge, and (iii) the shape of the perturbation. These three features are functions of NP concentration, structure-activity relations, UME size, reactant concentration, applied potential at the UME, and surface characteristics of both the UME and NPs (pretreatment, roughness, capping agents, among others). [87]

As an example of the importance of these parameters, NP particle sizing with nano-impacts has been shown to be a relevant characterization technique. The results of this new analytical technique are comparable to those obtained with vacuum and colloidal techniques.[37] Nano-impact has proven robust and reproducible for some specific NPs, with the main standard systems being Ag NP oxidation. Other metal NPs characterized are Au and Pt NP by electrocatalytic amplification. [42,83,87,96-98]

Current trace. The size and shape of the transients yield information about the interaction mechanisms. NPs have shown two types of response assigned depending on the adsorption time and the nature of the interaction with the UME. On the one hand, the step transient occurs when a NP adsorbs to the electrode over a longer period of time. Furthermore, the concentration of the particles is set low to avoid electrode saturation (no more than one collision at a time and a single NP layer; based on Poisson probability) [82, 83] and to allow the collection of multiple collisions over the experimental time. On the other hand, blip response occur when

J. Mex. Chem. Soc. **2023**, *67*(4)
Special Issue

ISSN-e 2594-0317

the adsorption of the NP is reversible, either the NP reacts on the UME or its surface does not interact with that of the UME.[87] In addition to nanoparticle collisions, blips can also arise from nanoparticle deactivation (poisoning) or if the NP material is modified (electrolyzed or electrotransformed). We can explain these two types of collisions by modeling them with an adsorption constant, as demonstrated in the mathematical derivation by Bard and coworkers [76]. If the adsorption of the NP is not fast enough, a more general equation can be written equation 13, which contemplates an adsorption constant: [76]

$$f_{p,ads} = k_{ads} C_{NP}^{pca} A \tag{13}$$

The kinetic constant of adsorption is related to that of collisions by a parameter that represents the probability of a collision resulting in adsorption, p_{ads}, by the actual rate of collisions, k_{coll}, which implies that not all collisions result in an adsorption:[76]

$$k_{ads} = p_{ads} k_{coll} \tag{14}$$

This boundary condition implies that adsorption cannot happen unless there is a collision Thus, considering the concentration change in the frequency of collision equation (9) as a concentration gradient from the bulk of the suspension and the electrode surface, Bard and co-workers obtained equation 15: [76]

$$f_{p,d} = Am\left[C_{NP}^{*} - C_{NP}^{pca}\right] \tag{15}$$

Combining equations 13 and 15 and making the concentration at the electrode surface $C_{NP}^{pca} = 0$, for the electrode acting as a NP sink yields equation 16.

$$f_{p,d} = \frac{AmC_{NP}^{*}}{\left(1 + \frac{m}{k_{ads}}\right)} \tag{16}$$

In the limiting case where the adsorption constant is large the collision frequency will be that for the sticking collisions, only step transients, equation 9. Thus, equation 16 could be used to explain cases where the frequency of collisions is different from the diffusion-limited conditions. However, this equation is rarely used in the literature, likely because it is challenging to measure k_{ads} in eq. (16). Also, it is difficult to experimentally change some of the parameters systematically, such as in the case of electrode radius or area, A. Besides the adsorption mechanism, there are two other topics related to the NP collisions which are the colloid chemistry and the interface of the UME/NP: agglomeration and tunneling effects, respectively.

Agglomeration and aggregation

Most of the single particle experiments rely on colloidal NP suspensions, either because the electrochemical experiments involve the electrode immersed in the colloid, or because a colloid is used to disperse NP on a substrate. Because of this higher order structures, agglomerates and aggregates complicate the analysis of collision data as discussed by several authors.[32-37, 99] IUPAC recommends distinguishing between agglomerates and aggregates based on the interactions that give rise to these structures. An agglomerate is a cluster held together by physical interactions that can be dispersed, while particles bonded through chemical bonds form an aggregate. [100] Another related issue is colloidal stability, which is usually defined as the tendency of the particles to stay suspended without precipitation. [101]. Therefore, a colloid is unstable if the collisions between the suspended particles result in agglomeration of aggregation; in general, the formation of higher order structures is called coagulation or flocculation. In practice, the zeta potential for colloidal suspension is used to describe the stability that results from van der Waals and other attractive forces being countered by electrostatic repulsions. The overall theory that describes the stability as a net sum of the attractive and repulsive forces is the DLVO theory (named after Boris Derjaguin and Lev Landau, Evert Verwey and Theodoor Overbeek). [102] Interestingly, the zeta potential, ζ, is usually $|\zeta| < 100$ mV and is more relevant to

J. Mex. Chem. Soc. **2023**, *67*(4)
Special Issue

ISSN-e 2594-0317

the stability of the suspensions and the surface charge of particles larger than ca. 100 nm diameter. [103]. Therefore, at smaller NP sizes, the DLVO theory have limitations, and this corresponds to region of interest for its electrochemical reactivity. These issues explain some of the experimental limitations in NP electrochemistry: the colloid concentrations and the electrolyte concentration must be controlled to prevent agglomeration. Usually, supporting electrolyte concentration is < 10 mM and 1:1 electrolytes are preferred. For smaller NPs, steric stabilization means resorting to capping agents that can introduce tunneling complications.

Besides DLVO theory, other approaches have been proposed, such as the potential mean force (PMF) for nanostructures, although at the expense of extensive computation time. [37] More recently, a complementary treatment that centers in the entropy of mixing has been introduced by Compton and coworkers [37]. This model includes a thermodynamic view on reversible agglomeration and is based on general statistical thermodynamics using the mixing entropy and the enthalpy of agglomerate formation as the main concepts which implies the agglomeration to be a reversible process taking place in stable suspensions.

The agglomeration approach taken by Sokolov et al. [37] shows a reasonable agreement between theory and experiments. As it can be seen from Fig. 3**(a)**, the mixing entropy results in distributions closer to lognormal size distributions for the suspensions. On the other hand, the function for interactive NPs (aggregates) can be described only if the enthalpy model is adjusted from the experimental results considering all possible aggregates and connection states, but the authors did not attempt this calculation because the complexity of finding a suitable model. Finally, the authors validated the model of the weakly interactive system with citrate-capped silver NPs system of 100 nm diameter, as shown in Fig. 3**(b)**. Furthermore, colored line-traces are related to the contribution of each individual agglomeration states to the overall distribution, which shows good agreement with the histogram. The contribution of different clusters, as shown in Fig. 3**(b)**, will shift the overall distribution towards a log-normal type and mainly experimental data of agglomerating systems typically show system with no larger clusters than 6 particles agglomerating. [37] This analysis of lognormal distribution can be applicable to a variety of system even the highly interactive ones as TiO_2 [35,75] and ZnO [33] NPs studies.

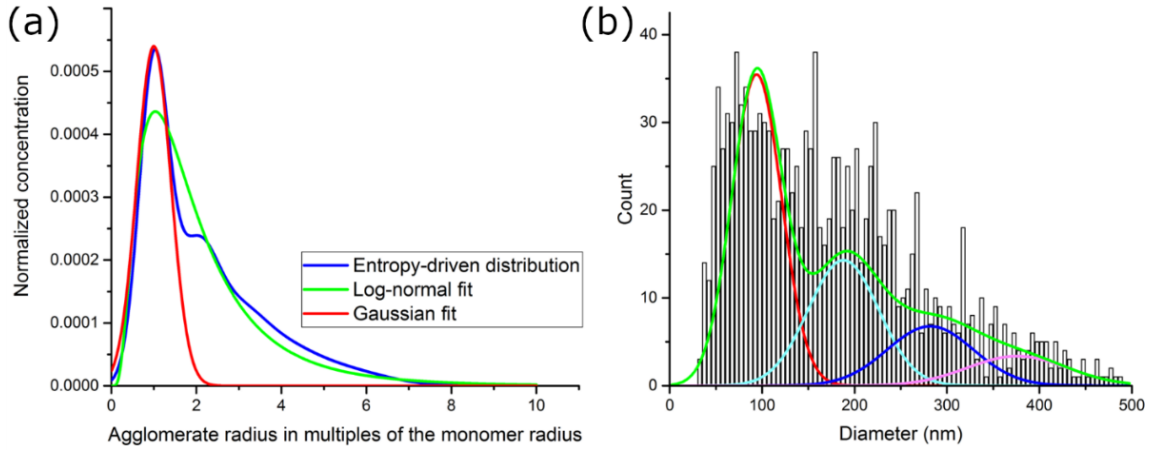

Fig. 3. Agglomeration studies **(a)** fitting distribution compared to entropy-driven process, and **(b)** size distribution comparison with experimental histogram from Nanoparticle Tracking Analysis, silver NPs of 100 nm diameter by TEM capped with citrate. Green trace is the distribution predicted via maximization of the entropy, red monomer, cyan dimer, blue trimer, and pink tetramer. Adapted with permission *J. Phys. Chem. C.* **2015**, *119* (44), 25093–25099, American Chemical Society.

Electron tunneling

Previous sections focused on the ideas of NPs diffusing in a Brownian motion and how NPs agglomerate before reaching the plane of closest approach. However, either a monomer or a cluster of NPs will interact with the electrode and adopt the electrode potential as it approaches the electrode and it is within tunneling distance, and during the time of the impact or adsorption. While the possibility of tunneling between the electrode and NP

J. Mex. Chem. Soc. **2023**, *67*(4)
Special Issue

ISSN-e 2594-0317

has been recognized for some time [104-109], Kätelhön and Compton recently addressed the issue with an equivalent circuit that allowed them to model the tunneling distance and the effect on potential and the NP electrochemistry. [110] We note that NP/electrode interaction could be more complex, due to the catalytic activity of the NP, the chemistry of the NP (electrolysis), blocking the electrode surface or a combination of any of these processes. The nature of the collision response, in the current versus time curve, will determine the observed transient if the potentiostat's resolution is enough to resolve the entire process. However, faster processes such as surface reactions, fast adsorption, and linkage of the NP is most probably hidden by the present-day resolution of instruments that only allow to measure events in the time domain down to ca. 30 µs. [82,85,111]

Kätelhön and Compton developed a theoretical model to describe the charge transfer process during nano-impacts. [110] Particles will behave as a nanoelectrode in the case of conductor materials. Either by a Faradaic interaction or mediating the current between the electrode and the solution, more general, the condensed phase in a pure colloidal system. The former is modeled as a classical reversible behavior of an electrode where reactions will occur on surface of the particle. The electron transfer process can happen by an antenna effect due to electron tunneling in an agglomerate or aggregate net [112,113]. These electrochemical processes could happen even when there is no connection (adsorption) between the UME and particle hence, it will be a function of the electrode-particle distance. In the Kätelhön and Compton model, the electron transfer was found to switch from a limiting Faradaic current and no current as a function of the electrode-particle distance, within a range of 0.2 nm. Fig. 4 depicts the model based on an equivalent circuit where tunneling and charge transfer are represented by resistances: the Ohmic tunneling resistance, R_t, and, the Ohmic Faradaic interface resistance, R_i. These two resistances describe the current due to charge transfer across the electrochemically active nanoparticle (in contact) or inactive, far from the surface, at the bulk solution potential. The bulk potential, E_{bulk}, is set to be $E_{bulk} = 0\,V$, and this corresponds to an equilibrium potential between species A and B in the colloid where there is no reaction on the suspended NP. Thus, E_{bulk} = 0 V corresponds to a certain A/B concentration, negative of the formal potential, $E^{0'}$, of the redox couple: B + e = A. The UME electrode potential is E_{el}, and is set to +1.0 V, so that a net oxidation of A occurs:

$$A \rightleftharpoons B + e \tag{17}$$

Note that as before, the substrate is inert and only the NP is capable of mediating eq (17).

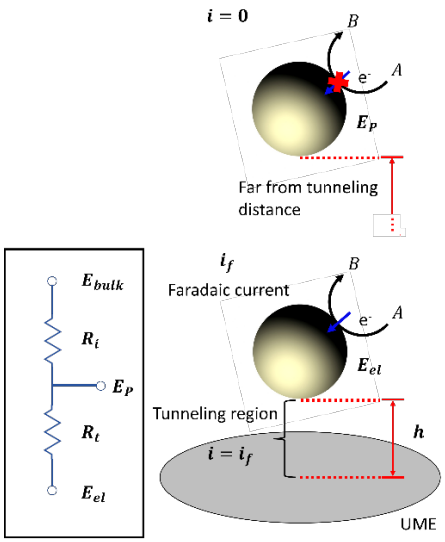

Fig. 4. NP charge transfer model includes a faradic current and a resistance to account for tunneling effects. **(a)** equivalent circuit and **(b)** schematics of the tunneling interaction. Adapted with permission from ChemElectroChem, 2015, 2: 64-67. Copyright 2014, John Wiley and Sons.

J. Mex. Chem. Soc. **2023**, *67*(4)
Special Issue

ISSN-e 2594-0317

The electrochemical reaction mediated by the NP is modeled as a diffusional steady-state current due to the size of the NP, equation 18, which corresponds to the shape of the reversible voltammogram: [110]

$$R_i = \frac{E_p}{I_f} = \frac{E_p}{I_{lim}}\left\{1 + exp\left[-\frac{F}{RT}\left(E_p - E^{0\prime}\right)\right]\right\} \quad (18)$$

Where E_p is the particle potential, I_f is the Faradaic current across the particle surface, I_{lim} is the limiting Faradaic current, and $E^{0\prime}$ is the formal potential of the electroactive species reacting at the surface of the particle, as above. F, R, and T are the Faraday constant, the universal gas constant, and the temperature, respectively. The authors used Simmons' tunneling equation [114] across a potential barrier to derive eq. (19): [110].

$$R_t = \frac{E_{el}}{I_t} = \frac{h}{C_1} exp(\kappa h) \quad (19)$$

Where E_{el} is the electrode potential, I_t is the tunneling current, h is the distance between the surface of the NP and the electrode surface, and C_1 and κ are experimental constants. Kätelhön and Compton estimated values for C_1 and κ. Finally, to perform numerical simulations of the tunneling process in order to model the effect E_p, $E^{0'}$, and tunneling distance, h, , they combined equations (18) and (19), and simulated the NP current for selected values of $E^{0'}$ within the domain of $0\ V \leq E_p \leq E_{el}$ with $E_{el,} = 1\ V$ and $0\ V \leq E^{0'} \leq 0.4\ V$, and $0\ \leq h\ \leq 2\ nm$. Their simulations indicate that as the particle approaches the electrode, the potential changes from E_{bulk} = 0 V to E_{el} = 1 V within 2 nm. However, the current changes from 0 to the limiting value, I_{lim}= 1 nA within approximately 1 nm of the surface, with most of the change happening within a range of 0.2 nm. This sharp change in current with distance led them to conclude that charge transfer has an on/off "binary nature". [110] This would simplify data analysis and simulations of future experiments, if the this binary nature is also present in different experiments that do not conform to all the assumptions made in the derivation of this model.

Summary

Although agglomeration and electron tunneling might seem unrelated at first, they illustrate the need to continue to work on single entity electrochemistry. Agglomeration is a day-to-day problem for colloidal scientists, that struggle to use the full surface area of catalysts in a nanoparticle. In single particle electrochemistry, minimizing agglomeration simplifies the data treatment, but it is possible that single entity experiments will provide new insights into agglomeration and its effect on mass transport or material deactivation. The second process, tunneling, corresponds to quantum phenomena observed in experiments and theory in other areas of physicalchemistry. In single entity experiments, we should be able to investigate the details of this nanoscale process, and in principle relate it to mesoscopic domain phenomena. However, our current instrumentation limits our ability to resolve details of the NP/electrode and NP-NP interactions. On the other hand, routine studies at the single NP level could help study the effect of structure on electrochemical reactivity, including the effect of capping agents, that also influence electrode/NP tunneling and NP agglomeration in suspensions. These experiments could guide the optimization of heterogeneous catalysis. Stochastic electrochemistry in the electrocatalytic amplification and some of its challenges could addresses several areas of technological relevance like sensors, with the possibility of using particles as tags, analogous to the optical methods used in ELISA methods. Studies of nucleation and growth at the single NP level [115-117] could lead to the possibility of making one particle at a time and possibly, yield automated routines to create nanostructures designed for specific functions. Overall, single entity studies may help us understand electrochemistry at the nanoscale.

J. Mex. Chem. Soc. **2023**, *67*(4)
Special Issue

ISSN-e 2594-0317

Acknowledgements

This paper is dedicated to Dr. Ignacio González Martínez as part of the JMCS special issue honoring the contributions of Drs. Elsa Arce Estrada, Joan Genescá Logueras, Ignacio González Martínez, Jorge Ibañez Cornejo, Yunni Meas Vong, and Omar Solorza Feria, because of their selection as emeriti members of the Mexican National System of Researchers (SNI for the Spanish acronym) emeritus status. We dedicate this paper to Dr. Ignacio González to celebrate his selection as SNI Emeritus and his National Mexican Electrochemical Society Award for his career-long contributions to electrochemistry in 2022. In addition, our group will submit a separate manuscript in honor of Dr. Jorge Ibáñez, who shared both distinctions with Dr. González.

We acknowledge support from the USA's National Science Foundation (NSF). This material is based upon work supported by the NSF under Grant No. 2108462.

References

1. Huang, K.; Shin, K.; Henkelman, G.; Crooks, R. M. *ACS Nano.* **2021**, *1*, 17926–17937.
2. Baker, L. A. *J. Am. Chem. Soc.* **2018**, *140*, 15549–15559.
3. *Faraday Discuss.* **2016**, *193*, 553–555.
4. Neher, E.; Sakmann, B. *Nature* **1976**, *260*, 799–802.
5. Fink, C. G.; Prince, J. D. *Trans. Am. Electrochem. Soc.* **1929**, *54*, 315.
6. Kamat, P. V. *J. Chem. Soc. Faraday Trans. 1 Phys. Chem. Condens. Phases.* **1985**, *81*, 509.
7. Koelle, U.; Moser, J.; Graetzel, M. *Inorg. Chem.* **1985**, *24*, 2253–2258.
8. Dunn, W. W.; Aikawa, Y.; Bard, A. J. *J. Am. Chem. Soc.* **1981**, *103*, 3456–3459.
9. Heyrovsky, M.; Jirkovsky, J.; Mueller, B. R. *Langmuir.* **1995**, *11*, 4293–4299.
10. Heyrovsky, M.; Jirkovsky, J.; Struplova-Bartackova, M. *Langmuir.* **1995**, *11*, 4300–4308.
11. Heyrovsky, M.; Jirkovsky, J.; Struplova-Bartackova, M. *Langmuir.* **1995**, *11*, 4309–4312.
12. Hellberg, D.; Scholfz F.; Schauer, F.; Weitschies, W. *Electrochem. Commun.* **2002**, *4*, 305–309.
13. Fan, F.-R. F.; Bard, A. J. *Science (80-.).* **1995**, *267*, 871–874.
14. Quinn, B. M.; van't Hof, P. G.; Lemay, S. G. *J. Am. Chem. Soc.* **2004**, *126*, 8360–8361.
15. Xiao, X.; Bard, A. J. *J. Am. Chem. Soc.* **2007**, *129*, 9610–9612.
16. Kang, S.; Nieuwenhuis, A. F.; Mathwig, K.; Mampallil, D.; Kostiuchenko, Z. A.; Lemay, S. G. *Faraday Discuss.* **2016**, *193*, 41–50.
17. Byers, J. C.; Paulose Nadappuram, B.; Perry, D.; McKelvey, K.; Colburn, A. W.; Unwin, P. R. *Anal. Chem.* **2015**, *87*, 10450–10456.
18. Chen, Q.; McKelvey, K.; Edwards, M. A.; White, H. S. *J. Phys. Chem. C* **2016**, *120*, 17251–17260.
19. Sun, P.; Mirkin, M. V. *J. Am. Chem. Soc.* **2008**, *130*, 8241–8250.
20. White, H. S.; McKelvey, K. *Curr. Opin. Electrochem.* **2018**, *7*, 48–53.
21. Percival, S. J.; Zhang, B. *J. Phys. Chem. C* **2016**, *120*, 20536–20546.
22. Guo, Z.; Percival, S. J.; Zhang, B. *J. Am. Chem. Soc.* **2014**, *136*, 8879–8882.
23. Blanchard, P.-Y.; Sun, T.; Yu, Y.; Wei, Z.; Matsui, H.; Mirkin, M. V. *Langmuir.* **2016**, *32*, 2500–2508.
24. Sun, T.; Yu, Y.; Zacher, B. J.; Mirkin, M. V. *Angew. Chemie Int. Ed.* **2014**, *53*, 14120–14123.
25. Li, Y.; Cox, J. T.; Zhang, B. *J. Am. Chem. Soc.* **2010**, *132*, 3047–3054.
26. Georgescu, N. S.; Robinson, D. A.; White, H. S. *J. Phys. Chem. C* **2021**, *125*, 19724–19732.
27. Zhou, M.; Yu, Y.; Hu, K.; Xin, H. L.; Mirkin, M. V. *Anal. Chem.* **2017**, *89*, 2880–2885.
28. Glasscott, M. W.; Pendergast, A. D.; Goines, S.; Bishop, A. R.; Hoang, A. T.; Renault, C.; Dick, J. E. *Nat. Commun.* **2019**, *10*, 2650.
29. Pendergast, A. D.; Glasscott, M. W.; Renault, C.; Dick, J. E. *Electrochem. Commun.* 2019, 98, 1–5.

J. Mex. Chem. Soc. **2023**, *67*(4)
Special Issue

ISSN-e 2594-0317

30. Kim, J.; Dick, J. E.; Bard, A. J. *Acc. Chem. Res.* **2016**, *49*, 2587–2595.
31. Kim, B.-K.; Boika, A.; Kim, J.; Dick, J. E.; Bard, A. J. *J. Am. Chem. Soc.* **2014**, *136*, 4849–4852.
32. Robinson, D. A.; Kondajji, A. M.; Castañeda, A. D.; Dasari, R.; Crooks, R. M.; Stevenson, K. J. *J. Phys. Chem. Lett.* **2016**, *7*, 2512–2517.
33. Karunathilake, N.; Gutierrez-Portocarrero, S.; Subedi, P.; Alpuche-Aviles, M. A. *ChemElectroChem* **2020**, *7*, 2248–2257.
34. Fernando, A.; Chhetri, P.; Barakoti, K. K.; Parajuli, S.; Kazemi, R.; Alpuche-Aviles, M. A. *J. Electrochem. Soc.* **2016**, *163*, H3025–H3031.
35. Fernando, A.; Parajuli, S.; Alpuche-Aviles, M. A. *J. Am. Chem. Soc.* **2013**, *135*, 10894–10897.
36. Sokolov, S. V.; Tschulik, K.; Batchelor-McAuley, C.; Jurkschat, K.; Compton, R. G. *Anal. Chem.* **2015**, *87*, 10033–10039.
37. Sokolov, S. V.; Kätelhön, E.; Compton, R. G. *J. Phys. Chem. C.* **2015**, *119*, 25093–25099.
38. Zhou, Y.-G. G.; Rees, N. V.; Compton, R. G. *ChemPhysChem.* **2011**, *12*, 2085–2087.
39. Zhou, H.; Fan, F.-R. R. F.; Bard, A. J. *J. Phys. Chem. Lett.* **2010**, *1*, 2671–2674.
40. Haddou, B.; Rees, N. V.; Compton, R. G. *Phys. Chem. Chem. Phys.* **2012**, *14*, 13612.
41. Kim, J.; Kim, B.-K. K.; Cho, S. K.; Bard, A. J. *J. Am. Chem. Soc.* **2014**, *136*, 8173–8176.
42. Xiao, X.; Fan, F.-R. F.; Zhou, J.; Bard, A. J. *J. Am. Chem. Soc.* **2008**, *130*, 16669–16677.
43. Zhou, Y.-G.; Rees, N. V.; Compton, R. G. *ChemPhysChem.* **2011**, *12*, 2085–2087.
44. Wang, Q.; Bae, J. H.; Nepomnyashchii, A. B.; Jia, R.; Zhang, S.; Mirkin, M. V. *J. Phys. Chem. Lett.* **2020**, *11*, 2972–2976.
45. Ma, H.; Ma, W.; Chen, J. F.; Liu, X. Y.; Peng, Y. Y.; Yang, Z. Y.; Tian, H.; Long, Y. T. *J. Am. Chem. Soc.* **2018**, *140*, 5272–5279.
46. Colón-Quintana, G. S.; Clarke, T. B.; Dick, J. E. *Nat. Commun.* **2023**, *14*, 705.
47. Glasscott, M. W.; Pendergast, A. D.; Dick, J. E. *ACS Appl. Nano Mater.* **2018**, *1*, 5702–5711.
48. Pendergast, A. D.; Glasscott, M. W.; Renault, C.; Dick, J. E. *Electrochem. Commun.* **2019**, *98*, 1–5.
49. Toh, H. S.; Compton, R. G. *Chem. Sci.* **2015**, *6*, 5053–5058.
50. Kim, B.-K. K.; Kim, J.; Bard, A. J. *J. Am. Chem. Soc.* **2015**, *137*, 2343–2349.
51. Mathuri, S.; Zhu, Y.; Margoni, M. M.; Li, X. *Front. Chem.* **2021**, *9*.
52. Patrice, F. T.; Qiu, K.; Ying, Y.-L.; Long, Y.-T. *Annu. Rev. Anal. Chem.* **2019**, *12*, 347–370.
53. Ren, H.; Edwards, M. A. *Curr. Opin. Electrochem.* **2021**, *25*, 100632.
54. Cheng, W.; Compton, R. G. *TrAC Trends Anal. Chem.* **2014**, *58*, 79–89.
55. Anderson, T. J.; Zhang, B. *Acc. Chem. Res.* **2016**, *49*, 2625–2631.
56. Alpuche-Aviles, M. A., in: *Encyclopedia of Electrochemistry*, Wiley, **2021**, 1–30.
57. Singh, P. S.; Lemay, S. G. *Anal. Chem.* **2016**, *88*, 5017–5027.
58. Sekretareva, A. *Sensors and Actuators Reports.* **2021**, *3*, 100037.
59. Gao, R.; Edwards, M. A.; Qiu, Y.; Barman, K.; White, H. S. *J. Am. Chem. Soc.* **2020**, *142*, 8890–8896.
60. Wahab, O. J.; Kang, M.; Unwin, P. R. *Curr. Opin. Electrochem.* **2020**, *22*, 120–128.
61. Dick, J. E.; Renault, C.; Bard, A. J. *J. Am. Chem. Soc.* **2015**, *137*, 8376–8379.
62. Kim, B.-K.; Boika, A.; Kim, J.; Dick, J. E.; Bard, A. J. *J. Am. Chem. Soc.* **2014**, *136*, 4849–4852.
63. Boika, A.; Thorgaard, S. N.; Bard, A. J. *J. Phys. Chem. B* **2013**, *117*, 4371–4380.
64. Zhou, Y.-G.; Rees, N. V.; Compton, R. G. *Angew. Chemie.* **2011**, *123*, 4305–4307.
65. Sokolov, S. V.; Tschulik, K.; Batchelor-McAuley, C.; Jurkschat, K.; Compton, R. G. *Anal. Chem.* **2015**, *87*, 10033–10039.
66. Jiao, X.; Lin, C.; Young, N. P.; Batchelor-McAuley, C.; Compton, R. G. *J. Phys. Chem. C* **2016**, *120*, 13148–13158.
67. Kätelhön, E.; Sepunaru, L.; Karyakin, A. A.; Compton, R. G. *ACS Catal.* **2016**, *6* , 8313–8320.

J. Mex. Chem. Soc. **2023**, *67*(4)
Special Issue

ISSN-e 2594-0317

68. Stockmann, T. J.; Angelé, L.; Brasiliense, V.; Combellas, C.; Kanoufi, F. *Angew. Chemie Int. Ed.* **2017**, *56*, 13493–13497.
69. Lin, C.; Sepunaru, L.; Kätelhön, E.; Compton, R. G. *J. Phys. Chem. Lett.* **2018**, *9*, 2814–2817.
70. Batchelor-McAuley, C.; Ellison, J.; Tschulik, K.; Hurst, P. L.; Boldt, R.; Compton, R. G. *Analyst.* **2015**, *140*, 5048–5054.
71. Zhang, F.; Edwards, M. A.; Hao, R.; White, H. S.; Zhang, B. *J. Phys. Chem. C* **2017**, *121*, 23564–23573.
72. Park, J. H.; Zhou, H.; Percival, S. J.; Zhang, B.; Fan, F. R. F.; Bard, A. J. *Anal. Chem.* **2013**, *85*, 964–970.
73. Zhou, H.; Park, J. H.; Fan, F. R. F.; Bard, A. J. *J. Am. Chem. Soc.* **2012**, *134*, 13212–13215.
74. Trojánek, A.; Mareček, V.; Samec, Z. *Electrochem. Commun.* **2018**, *86*, 113–116.
75. Fernando, A.; Chhetri, P.; Barakoti, K. K.; Parajuli, S.; Kazemi, R.; Alpuche-Aviles, M. A. *J. Electrochem. Soc.* **2016**, *163*, H3025–H3031.
76. Kwon, S. J.; Zhou, H.; Fan, F.-R. F.; Vorobyev, V.; Zhang, B.; Bard, A. J. *Phys. Chem. Chem. Phys.* **2011**, *13*, 5394.
77. Laborda, E.; Molina, A.; Espín, V. F.; Martínez-Ortiz, F.; García de la Torre, J.; Compton, R. G. *Angew. Chemie Int. Ed.* **2017**, *56*, 782–785.
78. Ortiz-Ledón, C. A.; Zoski, C. G. *Anal. Chem.* **2017**, *89*, 6424–6431.
79. Park, J. H.; Boika, A.; Park, H. S.; Lee, H. C.; Bard, A. J. *J. Phys. Chem. C* **2013**, *117*, 6651–6657.
80. Bobbert, P. A.; Wind, M. M.; Vlieger, J. *Phys. A Stat. Mech. its Appl.* **1987**, *141*, 58–72.
81. Zhou, Y.-G.; Rees, N. V.; Compton, R. G. *ChemPhysChem.* **2011**, *12*, 2085–2087.
82. Gutierrez-Portocarrero, S.; Sauer, K.; Karunathilake, N.; Subedi, P.; Alpuche-Aviles, M. A. *Anal. Chem.* **2020**, *92*, 8704–8714.
83. Little, C. A.; Xie, R.; Batchelor-McAuley, C.; Kätelhön, E.; Li, X.; Young, N. P.; Compton, R. G. *Phys. Chem. Chem. Phys.* **2018**, *20*, 13537–13546.
84. Oja, S. M.; Robinson, D. A.; Vitti, N. J.; Edwards, M. A.; Liu, Y.; White, H. S.; Zhang, B. *J. Am. Chem. Soc.* **2017**, *139*, 708–718.
85. Kanokkanchana, K.; Saw, E. N.; Tschulik, K. *ChemElectroChem.* **2018**, *5*, 3000–3005.
86. Fleischmann, M.; Oldfield, J. W. *J. Electroanal. Chem. Interfacial Electrochem.* **1970**, *27*, 207–218.
87. Kwon, S. J.; Zhou, H.; Fan, F. R. F.; Vorobyev, V.; Zhang, B.; Bard, A. J. *Phys. Chem. Chem. Phys.* **2011**, *13*, 5394–5402.
88. Robinson, D. A.; Liu, Y.; Edwards, M. A.; Vitti, N. J.; Oja, S. M.; Zhang, B.; White, H. S. *J. Am. Chem. Soc.* **2017**, *139*, 16923–16931.
89. Bard, A. J.; Faulkner, L. R.; White, H. S. 3rd ed.; Wiley, 2022.
90. Wightman, R. M.; Wipf. In: *Electroanalytical Chemistry*. Marcel Dekker, INC: New York, 1989; 267–353.
91. Wightman, R. M. *Anal. Chem.* **1981**, *53*, 1125A-1134A.
92. Saito, Y. *Rev. Polarogr.* **1968**, *15*, 177–187.
93. Heyrovský, J.; Ilkovič, D. *Collect. Czechoslov. Chem. Commun.* **1935**, *7*, 198–214.
94. Ilkovič, D. *Collect. Czechoslov. Chem. Commun.* **1934**, *6*, 498–513.
95. MacGillavry, D.; Rideal, E. K. *Recl. des Trav. Chim. des Pays-Bas.* **1937**, *56*, 1013–1021.
96. Ellison, J.; Tschulik, K.; Stuart, E. J. E.; Jurkschat, K.; Omanović, D.; Uhlemann, M.; Crossley, A.; Compton, R. G. *ChemistryOpen.* **2013**, *2*, 69–75.
97. Bartlett, T. R.; Sokolov, S. V.; Compton, R. G. *ChemistryOpen.* **2015**, *4*, 600–605.
98. Tschulik, K.; Haddou, B.; Omanović, D.; Rees, N. V.; Compton, R. G. *Nano Res.* **2013**, *6*, 836–841.
99. Kleijn, S. E. F.; Serrano-Bou, B.; Yanson, A. I.; Koper, M. T. M. *Langmuir* **2013**, *29*, 2054–2064.

J. Mex. Chem. Soc. **2023**, *67*(4)
Special Issue

ISSN-e 2594-0317

100. Alemán, J. V.; Chadwick, A. V.; He, J.; Hess, M.; Horie, K.; Jones, R. G.; Kratochvíl, P.; Meisel, I.; Mita, I.; Moad, G.; et al. *Pure Appl. Chem.* **2007**, *79*, 1801–1829.
101. Hunter, R. J. in: *Foundations of Colloid Science*. Oxford University Press: New York, **1992**.
102. Israelachvili, J. N. in: *Intermolecular and Surface Forces*. Academic Press: Burlington, MA, **2011**.
103. Morrison, I. D.; Ross, S. in: *Colloidal Dispersions: Suspensions, Emulsions, and Foams*. Wiley: New York, **2002**.
104. Lu, S.-M.; Peng, Y.-Y.; Ying, Y.-L.; Long, Y.-T. *Anal. Chem.* **2020**, *92*, 5621–5644.
105. Mirkin, M. V.; Sun, T.; Yu, Y.; Zhou, M. *Acc. Chem. Res.* **2016**, *49*, 2328–2335.
106. Lu, S.-M.; Chen, J.-F.; Wang, H.-F.; Hu, P.; Long, Y.-T. *J. Phys. Chem. Lett.* **2023**, *14*, 1113–1123.
107. Lu, S.-M.; Chen, J.-F.; Peng, Y.-Y.; Ma, W.; Ma, H.; Wang, H.-F.; Hu, P.; Long, Y.-T. *J. Am. Chem. Soc.* **2021**, *143*, 12428–12432.
108. Ma, W.; Ma, H.; Chen, J.-F.; Peng, Y.-Y.; Yang, Z.-Y.; Wang, H.-F.; Ying, Y.-L.; Tian, H.; Long, Y.-T. *Chem. Sci.* **2017**, *8*, 1854–1861.
109. Hill, C. M.; Kim, J.; Bard, A. J. *J. Am. Chem. Soc.* **2015**, *137*, 11321–11326.
110. Kätelhön, E.; Compton, R. G. *ChemElectroChem.* **2015**, *2*, 64–67.
111. Robinson, D. A.; Edwards, M. A.; Ren, H.; White, H. S. *ChemElectroChem.* **2018**, *5*, 3059–3067.
112. Wang, C.; Pagel, R.; Bahnemann, D. W.; Dohrmann, J. K. *J. Phys. Chem. B* **2004**, *108*, 14082–14092.
113. Wang, C.; Pagel, R.; Dohrmann, J. K.; Bahnemann, D. W. *Comptes Rendus Chim.* **2006**, *9*, 761–773.
114. Simmons, J. G. *J. Appl. Phys.* **1963**, *34*, 1793–1803.
115. Dick, J. E.; Hilterbrand, A. T.; Boika, A.; Upton, J. W.; Bard, A. J. *Proc. Natl. Acad. of Sci. U.S.A.* **2015**, *112*, 5303-5308. DOI: 10.1073/pnas.1504294112.
116. Dick, J. E.; Hilterbrand, A. T.; Strawsine, L. M.; Upton, J. W.; Bard, A. J. *Proc. Natl. Acad. of Sci. U.S.A*. *113*, 6403-6408. DOI: 10.1073/pnas.1605002113.
117. Glasscott, M. W.; Hill, C. M.; Dick, J. E. *J. Phys. Chem. C.* **2020**, *124*, 14380–14389.
118. Zhou, M.; Dick, J. E.; Bard, A. J. *J. Am. Chem. Soc.* **2017**, *139*, 17677–17682.
119. Vitti, N. J.; Majumdar, P.; White, H. S. *Langmuir.* **2023**, *39*, 1173–1180.